FULL PAPER

ADVANCED
OPTICAL
MATERIALS
www.advopticalmat.d

Check for
updates

Voltage-Controlled Dielectric Function of Bilayer Graphene

Shun Okano,* Apoorva Sharma, Frank Ortmann, Akira Nishimura, Christoph Günther, Ovidiu D. Gordan, Kenji Ikushima, Volodymyr Dzhagan, Georgeta Salvan,* and Dietrich R. T. Zahn

The refractive index and the extinction coefficient are usually inherent (noncontrollable) material characteristics. Recently, it was reported that the reflectivity of graphene in the mid-infrared spectral range can be modified by an external bias. This report attracted much attention, but the controllable frequency/energy range is too narrow for possible applications. In this work, it is demonstrated that the potential of graphene is not limited to mid-infrared wavelengths, but spans a much wider range including the visible spectral range. Here, back-gated bilayer graphene is characterized in air using spectroscopic ellipsometry with a lateral resolution in the micrometer range. By applying a back-gate voltage, the dielectric function can be modified in a broad spectral range, including the visible spectrum. To explain the change in the dielectric function, a simplified phenomenological approach which assumes that the back-gating-induced change in the carrier density of graphene can be described by a modified 2D Drude model is introduced. The trend of increasing values for the dielectric function with increasing sheet charge carrier density is confirmed by theoretical calculations performed in the independent particle picture.

1. Introduction

Graphene is currently one of the most intensively investigated carbon derivatives due to its unique properties like the linear energy dispersion at the *k*-point of the Brillouin zone and the presence of a 2D electron system.[1–3] Recently, it was demonstrated that due to interband transitions graphene strongly interacts with infrared (IR) light, making it a promising candidate for the detection and generation of IR/THz radiation.[4] Remarkably, the electronic structure of graphene can

be tailored from semimetallic to semiconducting by opening the zero bandgap, e.g., by applying an electric field,[5] chemical doping,[6] and/or strain,[7] offering opportunities for engineering its optical properties. Recently, Wang et al. reported strong and layer-dependent optical transitions of graphene and the tunability of reflectance in mid-infrared (MIR) by back-gating.[8] Polat and Kocabas reported a transmittance modulation of up to 35% in graphene supercapacitors working with ionic electrolytes in the spectral range from 500 to 1200 nm.[9]

The manipulation of the dielectric function of graphene in the visible to near-infrared (NIR) region of the electromagnetic spectrum has tremendous application potential in both industrial and fundamental research fields. For instance, graphene is a highly promising material for electro-optical modulators.[10] The application of such materials as antirefractive coatings can improve the performance of optical and optoelectronic devices by selectively eliminating unwanted reflections.[11] On the other hand, substrates with tunable optical properties are highly desirable for the detection of minute amounts of molecules by surface-enhanced Raman spectroscopy (SERS)[12] in disciplines ranging from physics to biomedicine.

In this work, we present the influence of field-effect doping on the optical properties of back-gated bilayer graphene in air in a broad spectral range, from NIR to visible. We elucidate that

S. Okano, A. Sharma, C. Günther, Dr. O. D. Gordan, Prof. G. Salvan, Prof. D. R. T. Zahn
Semiconductor Physics
Chemnitz University of Technology
Chemnitz 09107, Germany
E-mail: sok@accurion.com; salvan@physik.tu-chemnitz.de
Prof. F. Ortmann
Center for Advancing Electronics Dresden
Technische Universität Dresden
Dresden 01062, Germany

Prof. F. Ortmann
Department of Chemistry
Technische Universität München
Garching 85748, Germany
A. Nishimura, Prof. K. Ikushima
Department of Applied Physics
Tokyo University of Agriculture and Technology
2-24-16 Nakacho, Koganei, Tokyo 184-0012, Japan
Dr. V. Dzhagan
Institute of Semiconductor Physics
National Academy of Sciences of Ukraine
Kyiv 03028, Ukraine
Dr. V. Dzhagan
Physics Department
Taras Shevchenko National University of Kyiv
Kyiv 01601, Ukraine

**ADVANCED
SCIENCE NEWS**
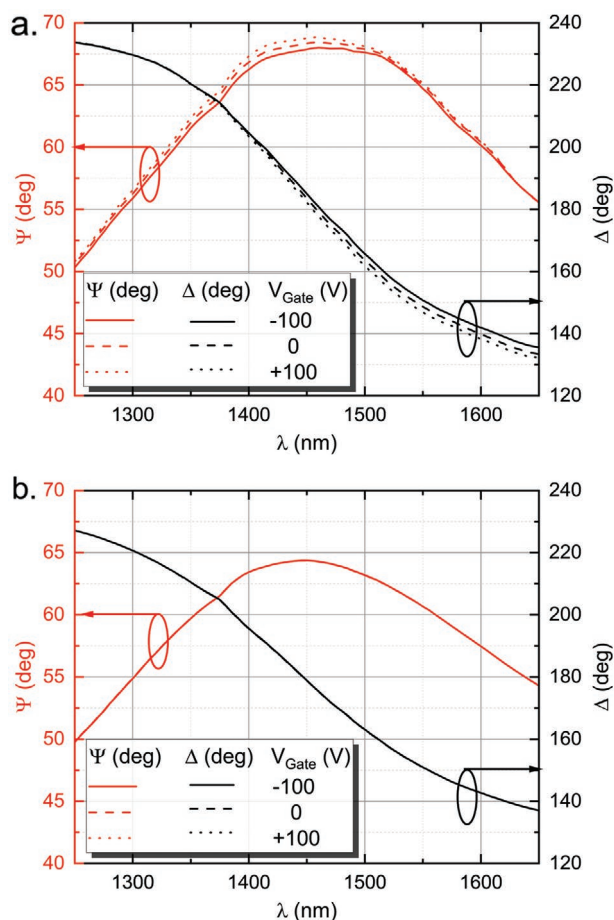www.advancedsciencenews.com

**ADVANCED
OPTICAL
MATERIALS**
www.advopticalmat.de

Figure 1. Ψ and Δ spectra of bilayer graphene a) and Si/SiO$_2$ substrate b). The red and black lines indicate experimental Ψ and Δ values at AOI of 55° with applied gate voltage −100, 0, and +100 V, respectively.

the change observed in the optical behavior cannot be explained by a simple Drude model, and hence, a modification of the Drude model for 2D systems is proposed.

2. Results and Discussion

The evolution in Ψ and Δ spectra as a function of wavelength and back-gate voltage measured on the bilayer graphene flake (**Figure 1**a) and on the substrate (Figure 1b) is shown in Figure 1. For ease of presentation, the spectra recorded at three applied back-gate voltages ($V_{Gate} = -100$, 0, and +100 V) are shown in the NIR region (full spectra are shown in Figure S2 in the Supporting Information). At first glance, it can be clearly observed that Ψ and Δ spectra measured on bilayer graphene change significantly according to the applied back-gate voltage. In contrast, no notable changes can be seen for the substrate Ψ and Δ spectra. Here it is worth mentioning that Si and SiO$_2$ are known to show the linear electro-optical effect (Pockels effect).[13,14] In the case of our sample, a layer of 300 nm SiO$_2$ is sandwiched between the highly conductive silicon substrate and the graphene flake acting as electrodes. Using the electro-optic coefficient from ref. [13] and following the procedure in

ref. [15], we estimated a change in refractive index of ≈10^{-5} due to the electro-optical effect of SiO$_2$ in the investigated voltage range. The resulting effects on the ellipsometric ψ and Δ spectra are below the detection limit of our ellipsometer. On the other hand, the highly doped silicon acts as an electrode and hence the voltage drop across the silicon substrate should be negligible, i.e., an electro-optical effect of the substrate can be excluded. This, in turn, implies that the optical properties of bilayer graphene are influenced by the back-gate voltage.

In order to emphasize the subtle spectral changes related to the field-effect doping so-called $\delta\Psi$ and $\delta\Delta$ difference spectra were calculated from the experimental data recorded at an angle of incidence (AOI) of 55° (see **Figure 2**a,b). Similar data recorded for other AOI are shown in the Supporting Information; see Figures S3 and S4 in the Supporting Information). The difference spectra were referenced to the spectra recorded at $V_{Gate} = 0$ V. A similar method was followed to calculate the difference spectra generated from the optical model (i.e., the fitted data). The spectral features observed at 310, 510, and 1410 nm for ψ and 305, 490, and, 1495 nm for Δ spectra are the combined effect of field-effect doping in bilayer graphene and strong interference conditions originating from the SiO$_2$ dielectric layer on the substrate.

Using the optical model described in Section 5, the ψ and Δ spectra were generated for each carrier concentration (corresponding to an experimentally applied voltage x). From each modeled ψ spectrum (respectively Δ spectrum), the ψ (Δ) spectra modeled for the carrier concentration corresponding to 0 V were subtracted in order to obtain the $\delta\psi$ ($\delta\Delta$) spectra, which are shown in Figure 2c,d

$$\delta\psi = \psi_{\text{model at } x \text{ Volt}} - \psi_{\text{model at 0 Volt}} \qquad (1)$$

$$\delta\Delta = \Delta_{\text{model at } x \text{ Volt}} - \Delta_{\text{model at 0 Volt}} \qquad (2)$$

The peaks observed in both modeled and experimental difference spectra originate from the constructive interference conditions of the substrate. These interference conditions subsequently enhance the changes in the measured Ψ and Δ spectra.

The thickness of the bilayer graphene and the energy position of the Van Hove singularity obtained from fitting, are $t_{\text{effective}} = (0.95 \pm 0.05)$ nm and ≈4.9 eV, respectively. These are in good agreement with previous studies of bilayer graphene, e.g., $t_{\text{bilayer graphene}} = 1.02$ nm[16] and $E_{\text{Van Hove}} = 4.6$ eV.[17,18] The resulting in-plane dielectric function (ε_1 and ε_2) obtained from regressive fitting is shown in **Figure 3**. A significant change (more than 50%) of in-plane dielectric function can be observed for longer wavelengths: at around 1400 nm the real part of the dielectric function ε_1 changes from 2.5 at $V_{Gate} = +100$, to 3.2 at 0 V, and to 4.0 at −100 V. Furthermore, for the same wavelength the imaginary part of the dielectric function ε_2 changes from 8.4 at +100, to 7.6 at 0 V, and to 7.1 at −100 V.

The n_{3D}, μ, and m^* values obtained from the fitting of the Drude oscillator are provided in **Table 1**. As stated above the n_{3D} carrier density obtained from the classical Drude model is valid for a 3D material. The approximate 2D carrier density was hence calculated from Equation (8). The values for the effective mass[19] of electrons in bilayer graphene obtained from
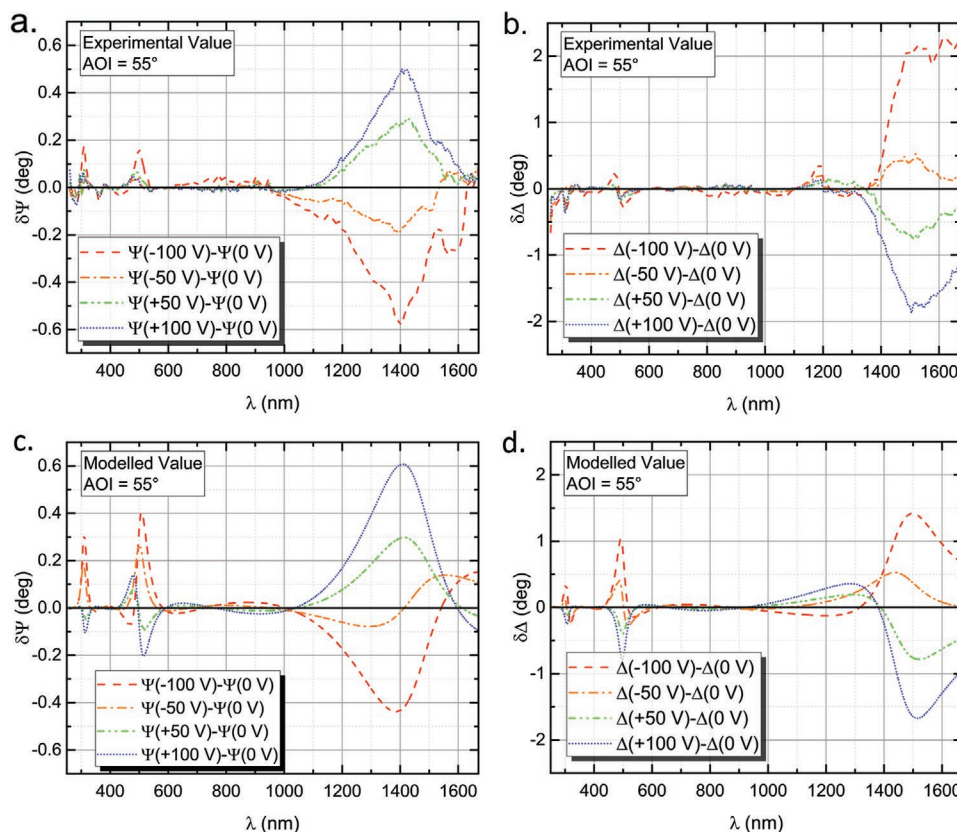
Figure 2. The difference spectra of bilayer graphene at AOI = 55° and various applied voltages with respect to $V_g = 0$ V: a,b) the experimental difference $\delta\Psi$ and $\delta\Delta$ spectra, and c,d) the modeled difference spectra.

the fitting are in the same order of magnitude as the values measured by the Hall effect ($m^* = 0.03 - 0.05$).[19] The values of the carrier mobility,[20] however, are one to two orders lower than the values measured in high vacuum using the Hall effect $\mu_{Vac} = (500 - 1000)$ cm^2 V^{-1} s^{-1}. This is likely due to the fact that the spectroscopic ellipsometry (SE) measurements here were performed in ambient conditions.

The influence of the gate voltage on the source–drain current is plotted in **Figure 4** (red curve). Under ideal conditions, the source–drain current minima should be centered at 0 V because the Fermi energy level (E_F) should be at the energy of the conduction band (CB) minimum and the valence band (VB) maximum. However, the observed offset suggests that our bilayer graphene is p-doped, resulting in E_F being shifted into the valence band. The cause of this effect is that the measurements were performed under ambient condition and some adsorbents from the air act as dopants. Therefore, a back-gate voltage of $V_{Gate} = +81$ V is required to bring E_F in the middle of CB and VB (minimum in a source–drain current curve). Changing the voltage around $V_{Gate} = +81$ V results in an increase or decrease of the carrier concentration, respectively. Moreover, the 2D carrier concentration obtained from SE as a function of applied back-gate voltage is also plotted in Figure 4. The black dashed line indicates a linear fit between $V_{Gate} = -100$ and +50 V, taking into account the positive carrier concentration. The slope of the fitted line $\frac{\Delta n_{2D}}{\Delta V} = -(6.7 \pm 0.2) \times 10^{10}$ cm^{-2} V^{-1}

is consistent with the expected rate of change of 2D carrier density per unit applied gate voltage[1,3] of $\pm (7.1 \times 10^{10})$ cm^{-2} V^{-1}. It should be mentioned that the main voltage drop occurs across the SiO$_2$ layer. The voltage drop across graphene is expected to be less than 0.01% of the applied voltage. Nevertheless, this voltage drop is sufficient to induce significant changes in the charge density in graphene, which in turn will influence the lineshape of the Drude oscillator and hence the dielectric function.

The DFT simulated dielectric function of the bilayer graphene with varying carrier concentration is shown in **Figure 5**a. The line shape of the simulated dielectric function is in very close agreement to the one obtained from the SE measurements. Similar to the SE obtained dielectric function, a monotonous increase in the absolute values can be observed in the calculated dielectric function with increasing carrier concentration. The magnitude of the simulated dielectric function was observed to be higher than the SE measured. This is largely due to the difference in the nominal thickness of bilayer graphene theoretical (2× monolayer) and experimental (cf. Equation (11)) of the graphene layer. Other aspects to be considered are the surface roughness and that the measurements were performed in ambient atmosphere, which is challenging to be considered precisely in the calculations. Notwithstanding, we find that both the theory and experimental results prove that the dielectric function of bilayer graphene can be manipulated under the influence of the back-gating, an effect which is due to the change in carrier concentration.
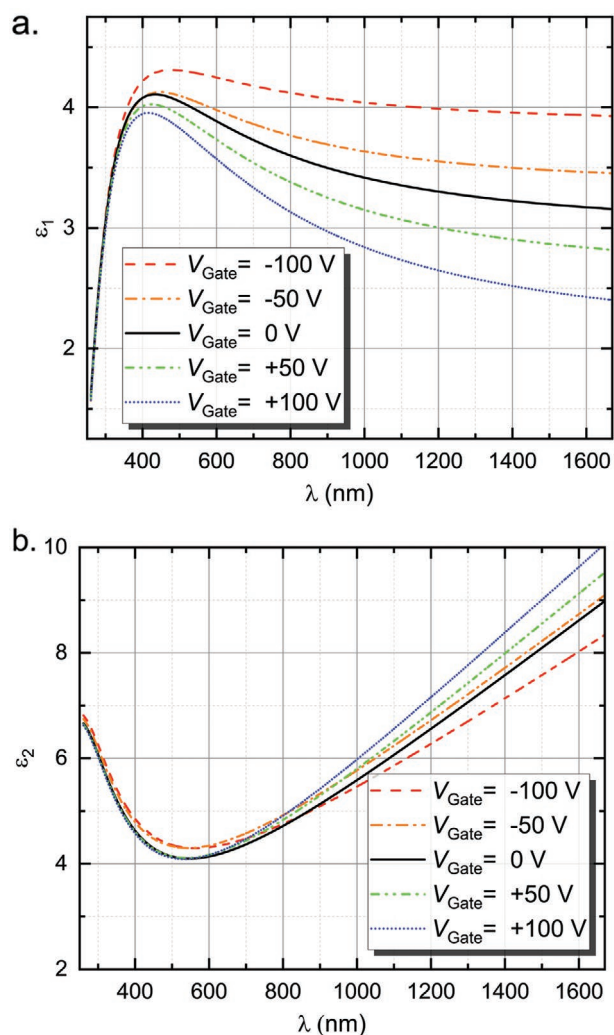
a.

b.

Figure 3. Real a) and imaginary parts b) of the in-plane dielectric functions of bilayer graphene as a function of back-gate voltage.

3. Conclusion and Perspectives

In this work, we demonstrate the control of the dielectric function of bilayer graphene in the visible and near-infrared spectral ranges by applying a back-gate voltage. Exfoliated bilayer graphene on a silicon substrate with 300 nm thermal grown SiO_2 was electrically contacted in a back-gate transistor geometry and investigated by spectroscopic ellipsometry in the NIR and visible spectral range while applying various gate voltages. The ellipsometric data were

Table 1. The Drude parameters derived from SE spectra for various applied back-gate voltages.

V_{Gate} [V]	$|n_{3D}|$ ($10^{20}cm^{-3}$)	$|n_{2D}|$ ($10^{13}cm^{-2}$)	μ [$cm^2 V^{-1} s^{-1}$]	$m*$
−100	2.68 ± 0.05	2.55 ± 0.19	18.52 ± 0.5	0.0156 ± 0.002
−50	2.31 ± 0.05	2.20 ± 0.17	23.92 ± 0.6	0.0147 ± 0.001
0	1.95 ± 0.04	1.85 ± 0.14	28.57 ± 0.8	0.0144 ± 0.0009
+50	1.63 ± 0.04	1.55 ± 0.13	36.68 ± 1	0.0121 ± 0.0006
+100	1.49 ± 0.02	1.41 ± 0.10	43.44 ± 2	0.0112 ± 0.0004

strongly influenced by the applied gate voltage, indicating a significant tuning of the dielectric constant ε_1 (e.g. from 2.5 to 4 at the wavelength of 1400 nm).

Theoretical calculations of the frequency-dependent dielectric function performed in the independent particle picture reproduce well the experimental trend of increasing values of the dielectric function with increasing sheet charge carrier density, while residual differences in the absolute values can be explained by the fact that the experiments were conducted under ambient atmosphere. To further explain the experimental observations, we introduced a phenomenological modified Drude approximation that takes into account the 2D character of graphene bilayer and allows the 2D carrier densities, mobilities, and effective masses to be determined. The obtained values are consistent with previously reported values for graphene.

The observation of such a significant tuning of the dielectric function in back-gated graphene in air demonstrates the robustness of the effect. Our approach of electrical tuning the dielectric function in the NIR and visible spectral range can be extended beyond graphene to any 2D material and paves the way toward the exploitation of the tunable optical properties of 2D materials in optoelectronics such as electro-optical modulators or antireflective coatings.

4. Experimental Section

Sample Preparation: The bilayer graphene sample was prepared by using the mechanical exfoliation technique. The exfoliated graphene flake was stamped on a highly n-doped Si substrate with a 300 nm thick thermally grown SiO_2 layer. The number of graphene layers was determined by Raman spectroscopy[21] (see Figure S1 in the Supporting Information) and the optical microscopic contrast technique.[22] Thereafter, the NiCr(10 nm)/Au(30 nm) electrodes were microfabricated using electron beam lithography (EBL). The details of the microfabrication process are reported elsewhere.[3]

Spectroscopic Ellipsometry: Spectroscopic ellipsometry measurements were conducted using an imaging ellipsometer Nanofilm EP4 from Accurion GmbH. The ellipsometer uses a laser stabilized xenon arc lamp as a light source followed by the monochromator with a single diffraction grating. The light reflected from the sample was collected with a microscope objective specially designed for spectroscopic measurement in a broad spectral range of λ = (260–1670) nm, 12.5 × magnification, a long working distance of 8.2 mm, and numerical aperture 0.25, with the proprietary name "Nanochromat." The collected light was then measured using a CCD detector. Such a configuration of optical components results in a lateral resolution of down to 2 µm and ensures a negligible misalignment in the angle of incidence (AOI) and angle of view (AOV) while maintaining the high lateral resolution. Due to its imaging capability with very high spatial resolution, the Nanofilm EP4 ellipsometer is proven to be useful for the spectroscopic analysis of flakes of 2D materials with a lateral size of only a few micrometers such as present in this work.

The ellipsometric angles Ψ and Δ are determined by measuring the complex ratio of Fresnel coefficients for s- and p-polarized light upon reflection from a sample surface

$$\rho = \frac{r_s}{r_p} = \tan(\psi)\,e^{i\Delta} \tag{3}$$

In this case, the spectral dependence of Ψ and Δ were measured for λ = (260–1670) nm at three angles of incidence (AOI) 50°, 55°, and 60°. All measurements were carried out under ambient

ADVANCED
SCIENCE NEWS
www.advancedsciencenews.com

ADVANCED
OPTICAL
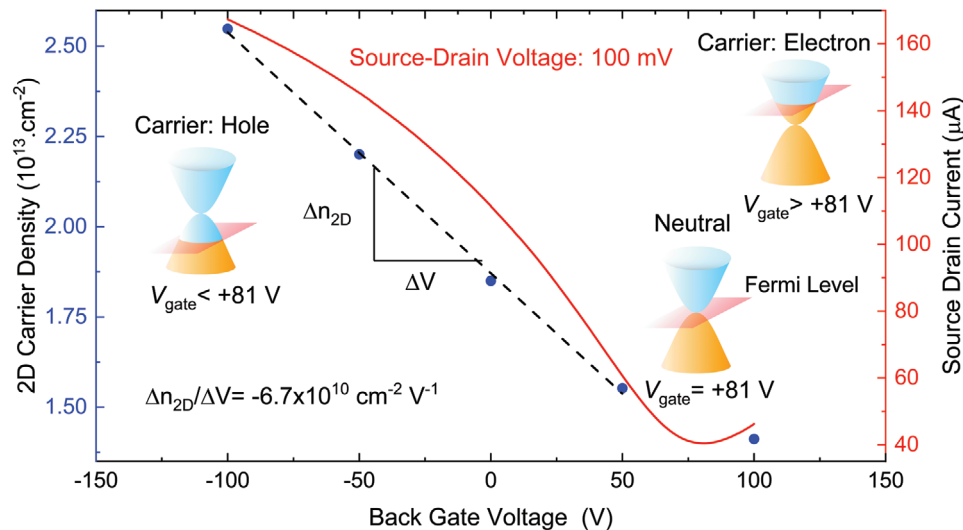MATERIALS
www.advopticalmat.de

Figure 4. The blue data points are the 2D carrier densities derived from the spectroscopic ellipsometry modeling, and the black dashed line is the linear fit through the data points. The red curve presents the analogous source–drain current as of the function of back-gate voltage.

conditions. The back-gate voltage-dependent Ψ and Δ spectra were recorded from the region of interest (ROI) marked in red in **Figure 6**b. for applied back-gate voltages of $V_{Gate} = -100, -50, 0, +50,$ and $+100$ V. Along with this, the Ψ and Δ spectra of the substrates were also recorded for each back-gate voltage by an ROI next to the graphene layer, shown as a blue box in Figure 6b. The data collected from the Si/SiO$_2$ (ROI in blue in Figure 6b) served for the purpose of reference measurements, to eliminate the influence of the experimental procedure (such as ROI drift under microscope objective and nonlinearity of optics and detectors) on the recorded spectra. The uncertainties in Ψ of $\leq 0.02°$ and Δ of $\leq 0.04°$ measurements were calculated from the standard deviation of Ψ and Δ obtained from repeated measurements.

Electrical Characterization: The electrical measurements were conducted on a homebuilt electrical test bench using a LabVIEW controlled Keithley 2636A source meter unit. For the measurement, a constant source–drain voltage of 100 mV was applied on the graphene and the source–drain current was monitored while sweeping the back-gate voltage from $V_{Gate} = -100$ to $+100$ V in steps of 1 V.

Data Analysis and Theory: In order to quantify the influence of the field-effect doping on the ellipsometric spectra, a layered-optical model consisting of the optical constant of Si[23] substrate followed by a Si/SiO$_2$ graded layer of 3.8 nm to emulate the intermixing between Si–SiO$_2$ and 303.2 nm thick SiO$_2$[23] on top. The precise thickness of SiO$_2$ was determined from the SE spectra recorded on the bare substrate (ROI in blue box cf. Figure 6). A GENOSC layer accounting for the optical constants of graphene, resembling the physical layer structure of the sample was designed. The GENOSC layer comprised a Drude oscillator to model changes in the spectra due to free charge carriers and a Lorentzian oscillator in order to take into account the Van Hove singularity in graphene. The summation of both Drude and Lorentzian contributions results in the overall dielectric function of graphene (Equation (4))

$$\varepsilon(E) = \varepsilon_1(E) + i\varepsilon_2(E) = \varepsilon_{Drude}(E) + \varepsilon_{Lorentz}(E) \tag{4}$$

where $\varepsilon(E)$ is the complex dielectric function of graphene, E is the photon energy, $\varepsilon_1(E)$ and $\varepsilon_2(E)$ are the real and imaginary parts of the dielectric function, respectively, and ε_{Drude} and $\varepsilon_{Lorentz}$ are the Drude and Lorentzian contributions to the dielectric function.

The Lorentz oscillator model is based on the classical theory of light–matter interaction and describes the photon energy-dependent electrical polarization of matter due to bound electrical charges

$$\varepsilon_{Lorentz}(E) = \frac{A\eta E_L}{E_L^2 - E^2 - iE\eta} \tag{5}$$

Here, A, η, and E_L denote the amplitude, the FWHM, and the centre energy position of the Lorentz oscillator, respectively.

The Drude theory is based on a free electron gas model and was developed for explaining the dielectric constants of metals.[24] Nevertheless, the theory can also be applied to nonmetallic materials with a high density of free charge carriers, including graphite and graphene[25–27]

$$\varepsilon_{Drude} = \varepsilon_0 \left\{ 1 - \frac{\omega_p^2}{\omega\left(\omega + \frac{i}{\tau}\right)} \right\} \tag{6}$$

where ω is the angular frequency of the electromagnetic wave, τ is the average time of the electron between scattering events, and ω_p is the plasma frequency of the system given by

$$\omega_p = \sqrt{\frac{ne^2}{m^*\varepsilon_0}} \tag{7}$$

where n is the carrier density, m^* is the effective mass of the charge carriers, e is the elementary charge of the electron, and ε_0 is the vacuum permittivity.

This model, however, treats an electron classically as a free particle in a constant potential and thus lacks the consideration of dimensionality of the sample under investigation. Therefore, the classical Drude model cannot be applied as such to describe charges in 2D systems. Here, a modified Drude approximation is proposed, which explains the experimental observations in 2D materials (on the example of graphene). To solve the problem mentioned above, it is assumed that the carrier concentration in a 2D system (n_{2D}) is proportional to the 3D carrier concentration (n_{3D}) and can be written as

$$n_{2D} = n_{3D} \cdot t \tag{8}$$

where t is the thickness of 2D material. Hence, the dielectric tensor of a 2D material can be written as follows
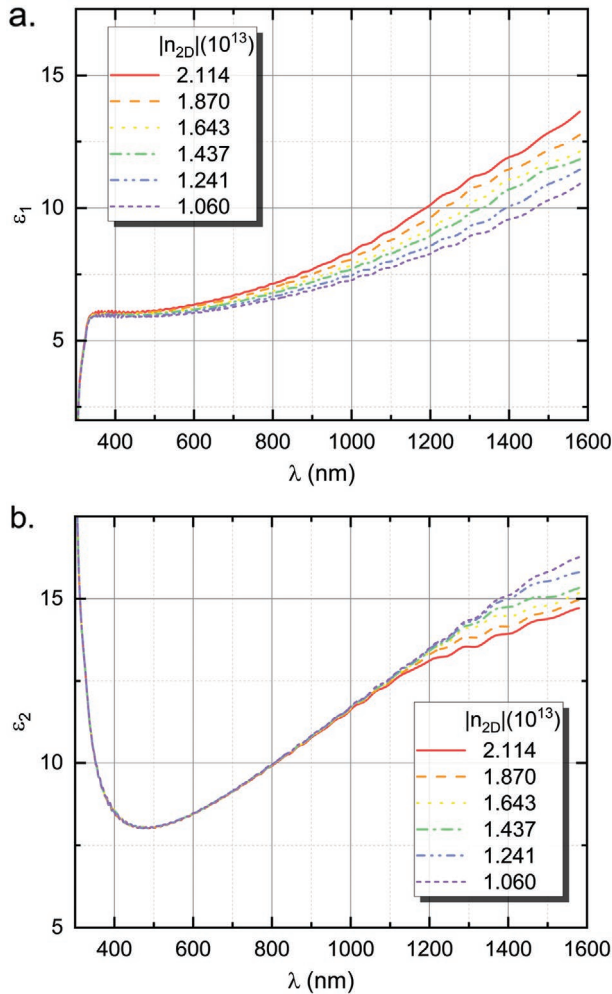
Figure 5. The DFT simulated real a) and imaginary b) parts of the dielectric function of bilayer graphene with various 2D carrier concentrations.

$$\varepsilon_{2D,\,Drude} = \varepsilon_0 \left\{ \begin{pmatrix} 1 & 0 & 0 \\ 0 & 1 & 0 \\ 0 & 0 & 1 \end{pmatrix} - \frac{\omega_{p2D}^2}{\omega\left(\omega + \frac{i}{\tau}\right)} \begin{pmatrix} 1 & 0 & 0 \\ 0 & 1 & 0 \\ 0 & 0 & 0 \end{pmatrix} \right\} \quad (9)$$

$$\omega_{p2D} = \sqrt{\frac{n_{2D} e^2}{m^* t \varepsilon_0}} \quad (10)$$

This model assumes the same effective electron mass in the 2D and 3D cases. Note that the z-component of the dielectric tensor is zero due to the confinement (lack of freedom) of electrons in the direction perpendicular to the graphene plane (xy). The charge carrier concentration obtained from the Drude model and its approximation in 2D will be referred to as n_{3D} and n_{2D}, respectively.

In order to implement the 2D Drude approximation in the optical model, the GENOSC layer was replaced with a uniaxial anisotropic material layer. The in-plane component (xy) of this uniaxial anisotropic layer represents the dielectric function of graphene defined above as the GENOSC layer (Drude and Lorentz oscillator), while the dielectric function of vacuum ($\varepsilon_1 = 1$, $\varepsilon_2 = 0$) was used as the out-of-plane (z) component.

For a more accurate characterization of the Ψ and Δ spectra recorded at various back-gate voltages, a multi-sample analysis approach was used. In this, the unknown parameters such as n_{3D}, μ, and m^* were kept as independent fit parameters for several ellipsometry spectra obtained by varying the back-gate voltage. The parameters of the Lorentz
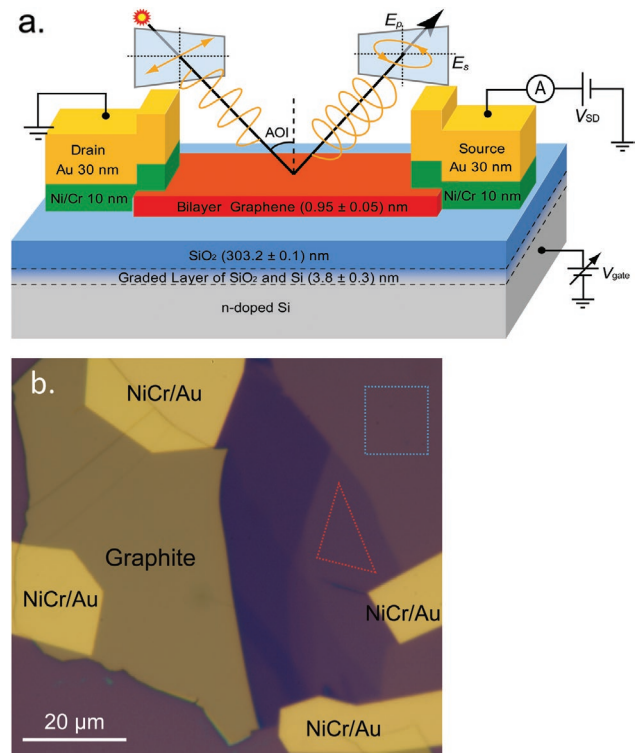

Figure 6. a) Schematic diagram of the sample and experimental setup. b) Optical image of the sample. The region enclosed in the red triangle shows bilayer graphene where the ellipsometry spectra were recorded, and the area bounded in the blue square was used for the ellipsometry characterization of the Si/SiO$_2$ (300 nm) substrate.

oscillator and the thickness were assumed not to be influenced under the application of back-gate voltage and can, thus, be determined unambiguously from the set of spectra recorded at various back-gate voltage. Here it should be noted that the thickness obtained from the SE analysis is an effective thickness ($t_{effective}$), which includes the thickness of bilayer graphene and an adsorbate layer due to the ambient conditions

$$t_{effective} = t_{bilayer\ graphene} + t_{adsorbent} \quad (11)$$

The fitting of the optical model to the measured data was performed using an iterative, nonlinear regression algorithm with the Complete EASE software provided by J. A. Woollam Co. Inc. In order to obtain an unambiguous solution for the correlated parameters (m^*, n_{2D}, etc.) multiple data sets generated from the variable angle spectroscopic measurement were fitted together. In addition, the fitting range for each parameter was set to a reasonable interval chosen based on reliable literature.[16–20]

Additionally, density functional theory simulations of freestanding bilayer graphene is performed in a slab geometry, where the distance between the two layers was fixed to $d = 3.355$ Å and the vacuum distance between periodic images was above 10 Å. Calculations were made using the code VASP,[28] where the electron–ion interaction was described by the PBE exchange-correlation functional[29] within the PAW scheme.[30,31] A dense grid of up to $450 \times 450 \times 1$ k-points was used for Brillouin-zone integration.

The frequency-dependent longitudinal dielectric function was calculated in the independent particle picture[32,33] because excitonic effects are expected to be weak.[34] A general expression for the tensor components of the dielectric function in the absence of local field effects is[35]

$$\varepsilon_{\alpha\beta}(\omega) = \delta_{\alpha\beta} + 4\pi^2 e_0^2 \sum_{c,v,k} \frac{2w_k}{\Omega} \frac{2}{\pi} \left\{ \frac{\varepsilon_{c,k} - \varepsilon_{v,k}}{\left[\varepsilon_{c,k} - \varepsilon_{v,k}\right]^2 - \left[\hbar\omega + i\eta\right]^2} \right\}$$
$$\times t_{vc\alpha}^*(k) t_{vc\beta}(k) \quad (12)$$

ADVANCED
SCIENCE NEWS
www.advancedsciencenews.com

ADVANCED
OPTICAL
MATERIALS
www.advopticalmat.de

with the matrix elements $t_{vc\beta}(\mathbf{k}) = \left[\langle v, \mathbf{k}+\mathbf{q} \,|\, \frac{\partial |c, \mathbf{k}+\mathbf{q}\rangle}{\partial q_\beta} \right]_{q=0}$ between valence (v) and conduction (c) bands calculated in the optical limit. $\varepsilon_{v,\mathbf{k}}$ and $\varepsilon_{c,\mathbf{k}}$ are the Kohn–Sham eigenvalues, $\eta = 0.04$ eV a broadening parameter and $w_\mathbf{k}$ the symmetry weight of the k-point in the irreducible Brillouin zone. The dielectric function was calculated with $\Omega = 2Ad$, with the lateral area of the primitive unit cell A and the bilayer thickness $2d$. The in-plane components are isotropic. The carrier density dependence of $\varepsilon_{\alpha\beta}(\omega)$ was obtained by the variable chemical potential that was used in Equation (12) to separate occupied and unoccupied states.

Conflict of Interest

The authors declare no conflict of interest.

[1] K. S. Novoselov, A. K. Geim, S. V. Morozov, D. Jiang, M. I. Katsnelson, I. V. Grigorieva, S. V. Dubonos, A. A. Firsov, *Nature* **2005**, *438*, 197.
[2] A. K. Geim, K. S. Novoselov, *Nat. Mater.* **2007**, *6*, 183.
[3] K. S. Novoselov, *Science* **2004**, *306*, 666.
[4] D. Yadav, S. B. Tombet, T. Watanabe, S. Arnold, V. Ryzhii, T. Otsuji, *2D Mater.* **2016**, *3*, 045009.
[5] Y. Zhang, T.-T. Tang, C. Girit, Z. Hao, M. C. Martin, A. Zettl, M. F. Crommie, Y. R. Shen, F. Wang, *Nature* **2009**, *459*, 820.
[6] H. Liu, Y. Liu, D. Zhu, *J. Mater. Chem.* **2011**, *21*, 3335.
[7] Z. H. Ni, T. Yu, Y. H. Lu, Y. Y. Wang, Y. P. Feng, Z. X. Shen, *ACS Nano* **2008**, *2*, 2301.
[8] F. Wang, Y. Zhang, C. Tian, C. Girit, A. Zettl, M. Crommie, Y. R. Shen, *Science* **2008**, *320*, 206.
[9] E. O. Polat, C. Kocabas, *Nano Lett.* **2013**, *13*, 5851.
[10] Z. Sun, A. Martinez, F. Wang, *Nat. Photonics* **2016**, *10*, 227.
[11] P. Spinelli, M. A. Verschuuren, A. Polman, *Nat. Commun.* **2012**, *3*, 692.
[12] T. Wang, Z. Zhang, F. Liao, Q. Cai, Y. Li, S.-T. Lee, M. Shao, *Sci. Rep.* **2015**, *4*, 4052.
[13] X.-C. Long, R. A. Myers, S. R. J. Brueck, *Opt. Lett.* **1994**, *19*, 1819.
[14] R. Soref, B. Bennett, *IEEE J. Quantum Electron.* **1987**, *23*, 123.
[15] J. A. Miragliotta, D. K. Wickenden, in *Gallium Nitride (GaN) II*, Vol. *57* (Eds: J. I. Pankove, T. D. Moustakas), Elsevier, Amsterdam **1999**, pp. 319–370.
[16] A. Gupta, G. Chen, P. Joshi, S. Tadigadapa, Eklund, *Nano Lett.* **2006**, *6*, 2667.
[17] V. G. Kravets, A. N. Grigorenko, R. R. Nair, P. Blake, S. Anissimova, K. S. Novoselov, A. K. Geim, *Phys. Rev. B* **2010**, *81*, 155413.
[18] A. H. Castro Neto, F. Guinea, N. M. R. Peres, K. S. Novoselov, A. K. Geim, *Rev. Mod. Phys.* **2009**, *81*, 109.
[19] W. Zhu, V. Perebeinos, M. Freitag, P. Avouris, *Phys. Rev. B* **2009**, *80*, 235402.
[20] K. Zou, X. Hong, J. Zhu, *Phys. Rev. B* **2011**, *84*, 085408.
[21] D. Graf, F. Molitor, K. Ensslin, C. Stampfer, A. Jungen, C. Hierold, L. Wirtz, *Nano Lett.* **2007**, *7*, 238.
[22] H. Li, J. Wu, X. Huang, G. Lu, J. Yang, X. Lu, Q. Xiong, H. Zhang, *ACS Nano* **2013**, *7*, 10344.
[23] C. M. Herzinger, B. Johs, W. A. McGahan, J. A. Woollam, W. Paulson, *J. Appl. Phys.* **1998**, *83*, 3323.
[24] P. Drude, *Ann. Phys.* **1900**, *306*, 566.
[25] U. Wurstbauer, C. Röling, U. Wurstbauer, W. Wegscheider, M. Vaupel, P. H. Thiesen, D. Weiss, *Appl. Phys. Lett.* **2010**, *97*, 231901.
[26] B. Kwiecinska, D. G. Murchison, E. Scott, *J. Microsc.* **1977**, *109*, 289.
[27] S. Ikeda, M. Yamashita, C. Otani, in *2014 39th Int. Conf. on Infrared, Millimeter, and Terahertz waves (IRMMW-THz)*, Vol. *2*, IEEE, Tucson, AZ **2014**, pp. 1–2.
[28] G. Kresse, J. Furthmüller, *Phys. Rev. B: Condens. Matter Mater. Phys.* **1996**, *54*, 11169.
[29] J. P. Perdew, K. Burke, M. Ernzerhof, *Phys. Rev. Lett.* **1996**, *77*, 3865.
[30] P. E. Blöchl, *Phys. Rev. B* **1994**, *50*, 17953.
[31] G. Kresse, D. Joubert, *Phys. Rev. B: Condens. Matter Mater. Phys.* **1999**, *59*, 1758.
[32] S. L. Adler, *Phys. Rev.* **1962**, *126*, 413.
[33] L. Matthes, P. Gori, O. Pulci, F. Bechstedt, *Phys. Rev. B: Condens. Matter Mater. Phys.* **2013**, *87*.
[34] L. Matthes, O. Pulci, F. Bechstedt, *New J. Phys.* **2014**, *16*, 105007.
[35] M. Gajdoš, K. Hummer, G. Kresse, J. Furthmüller, F. Bechstedt, *Phys. Rev. B: Condens. Matter Mater. Phys.* **2006**, *73*, 045112.